Experimental study of the geometrical barrier in type-I superconducting strips

H. Castro,* B. Dutoit,† A. Jacquier,‡ M. Baharami, and L. Rinderer
Institut de Physique Experimentale, Universite de Lausanne, CH-1015 Lausanne, Switzerland
(Received 22 July 1998)

We study the energy barrier for flux entry of a geometric origin in type-I superconducting strips using magneto-optical observations of the flux structure. The magnetic field is applied perpendicularly to the broad surface and, optionally, a dc current is sent along the strip. As a direct manifestation of this barrier, the appearance of flux-free zones at the edges of the strip is observed. The width of these zones, the field for first-flux penetration, and the critical current originated due to the geometrical barrier are measured. The dependence of these parameters on the geometry of the sample, applied field, transport current, and temperature presented here is in good qualitative agreement with a recent theory by Benkraouda and Clem.
[S0163-1829(98)05046-2]

I. INTRODUCTION

The study of different types of barriers, such as the Bean-Livingston, Gibbs free-energy, edge pinning, and geometrical barriers, in high-T_C superconductors has been the subject of recent works.[1–9] Interest in this subject arises from the need to understand the role played by each of them in different phenomena such as magnetization, flux relaxation, critical current, and hysteresis.[2,5–9] A geometrical barrier is generated due to the rectangular cross section and shape of the edges of the strip sample. We believe that a study of this barrier is possible in samples free of volumetric pinning and without surface and other types of defects. Single-crystalline type-I superconductors are therefore good candidates for this purpose.

Several authors have made measurements and calculations on type-I and -II superconducting strips; however, their interest was focused on other types of barriers or on other aspects of superconductivity.[3–4,10–12] Fortini *et al.*[13] pointed out the strong geometric influence of different Pb sample shapes (disks and deformed spheres) on the hysteresis observed in magnetization measurements. They presented an approach to the understanding of the geometrical barrier in type-I superconductors and found an expression for the threshold field H_p at which the flux penetration begins. Brandt and Indenbom[1] and Zeldov *et al.*[14] performed calculations and measurements of current and field distributions in type-II strips with a perpendicularly applied field and explained the origin of the geometrical barrier on the spatially distributed shielding current, due to the nonellipsoidal cross section of the strip. Their calculations, however, were done for samples with volumetric pinning and do not work in pinning-free ones. A calculation of current and field distributions in pinning-free type-II strips, without transport current, was performed by Zeldov *et al.*,[9] and a more detailed study was recently done by Benkraouda and Clem.[15] They discuss the possible configurations of the trapped flux with and without transport current, and the critical current originated on the geometrical barrier, thus providing a complete description of the geometrical barrier and some of its measurable manifestations.

This paper is organized as follows: The experiment and results are presented in Sec. II. In Sec. III we summarize the theoretical results from Ref. 15 needed for the discussion that follows in Sec. IV.

II. EXPERIMENT

A. Equipment for magneto-optical measurements

The experimental arrangement is schematically shown in Fig. 1. The magneto-optical (MO) indicator layer, deposited on the inner surface of a glass window (GW), lies at the bottom of the Dewar. The sample (S) is placed in close contact with the MO layer, immersed in a liquid He bath. The magnetic field is created by a Helmholtz field coil (FC). The optical system uses the rotation of the polarization axis of light with a magnetic field (Faraday effect). We work with the green line ($\lambda = 543$ nm) of a Hg lamp (Lp). After filtering (F), this light is sent through one of the optical paths of a

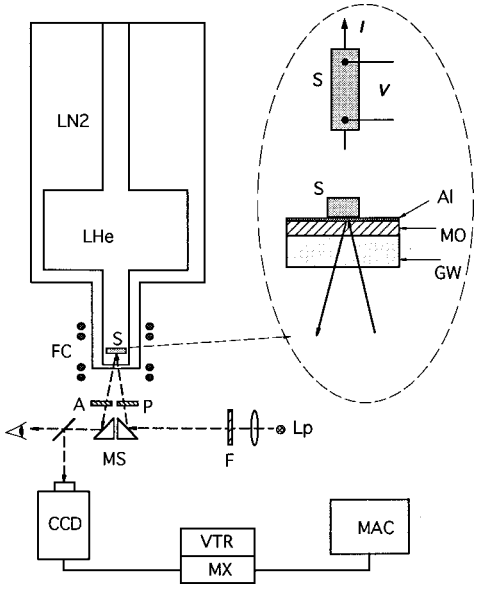

FIG. 1. Experimental setup for magneto-optical measurements: sample S, field coil FC, analyzer A, polarizer P, microscope MS, light filter F, Hg lamp Lp, magneto-optical indicator MO, aluminized surface Al, and glass window G.

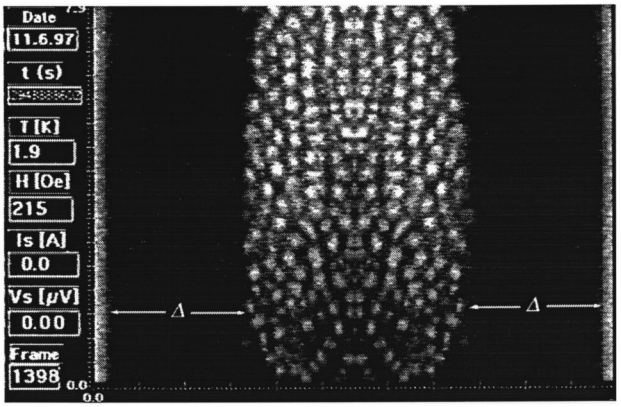

FIG. 2. Magneto-optical image of sample Pb3 for $I=0$ at 1.9 K. Flux structures are white and superconducting regions dark. The edges of the strip are indicated by the white lateral bands delimiting Δ.

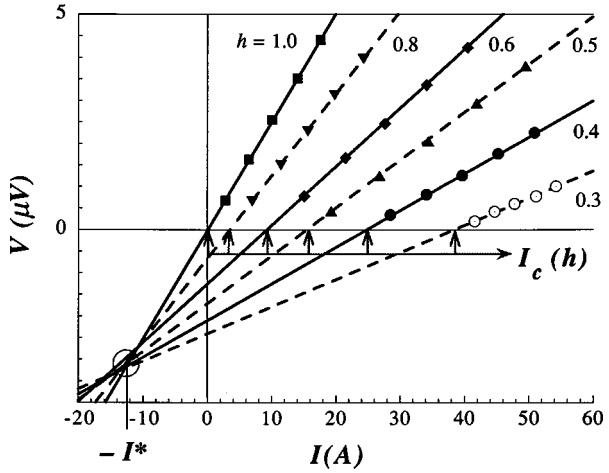

FIG. 3. V-I characteristics for sample Pb12 at 4.2 K. Here $I_c(h)$ is determined from the intersections with $V=0$. See the convergence point at $I=I^*$.

binocular microscope (MS), linearly polarized at (P), and then reflected on the aluminized surface (Al) of the indicator layer. After interacting with the field from the magnetic structure, the light rays return through the second optical path of the microscope and pass through the analyzer (A) to be focused, either on the ocular for direct observation, on a charge-coupled diode (CCD) camera for recording, or on a photographic camera. The temperature of the sample is adjusted by controlling the pressure of the LHe bath and monitored with a semiconductor thermometer.

The variables of interest, i.e., temperature T; current through the sample, I; voltage across the sample, V; applied field H_a; and time t, are continuously measured, mixed together (MX) with the corresponding images, displayed on a TV screen, and then recorded (VTR) on videotape for later analysis. The V-I measurements are obtained by the standard four-contact dc method.

Figure 2 shows a typical image where the flux-occupied regions are lighter than the dark flux-free zones. The edges of the strip are defined by the white bands delimiting the flux-free zones Δ, as indicated.

B. Samples

Single-crystalline strips were fabricated by pouring melted high-purity metal (Pb, In) onto a glass matrix under an inert Ar atmosphere. A high surface quality of samples is obtained by carbon-coating the glass surfaces so as to prevent the adherence of the metal. The matrix is then slowly displaced in a region with a temperature gradient from 10° above, down to 10° below, the melting point of the metal, in a process that takes about 8 h. Some of the samples were then electrochemically polished. Table I shows a list of selected samples with some of their characteristics.

EuSe indicator films, which determine the rotation of the polarization axis of light, were developed in our laboratory.[16,17] They were evaporated on special glass (SF-57) with a negligible optical reaction to mechanical stresses. The thickness of the films, typically 300 nm, is such that the antireflection condition is fulfilled, i.e., thickness$=m\lambda/4n$, where n is the refraction index, λ the light wavelength, and $m=5,7,9,...$, in order to enhance the Faraday effect.[18] The glass support serves at the same time as a window, separating the liquid He from the vacuum.

TABLE I. Sample characteristics.

Sample name	Width×thickness (mm^2)	$R(300\text{ K})/R(4\text{ K})$ (Ω/Ω)	Remarks
Pb2	3.10×0.50	2005/0.196	rectangular edges
Pb3	3.10×0.36	2801/0.3459	rectangular edges
Pb4	2.82×0.22	5213/0.5817	rectangular edges
Pb5	3.08×0.61	1619/0.1488	rectangular edges
Pb7	2.73×0.41	2569/0.2774	rectangular edges
Pb10	3.15×0.50		rectangular edges
Pb12	2.90×0.22		rectangular edges
Pb14	2.25–3.87×0.50[a]	1913/0.3243	beveled 30°, both sides
Pb15	2.65–3.43×0.50[a]	1934/0.1971	beveled 30°, one side
Pb16	3.00×0.50	1989/0.2610	rectangular edges
In105	3.00×0.20	2113/0.1400	rectangular edges
Hg	∅20.0×0.50		disk of diameter ∅

[a]The two widths in beveled samples correspond to the top and bottom faces.

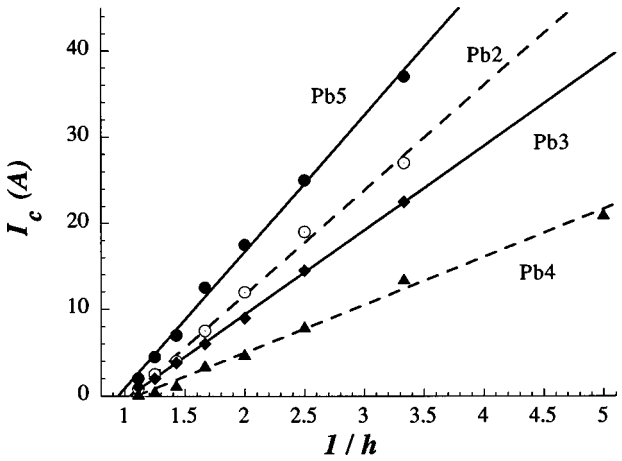

FIG. 4. I_c vs $1/h$ for Pb samples at 4.0 K. The lines are fits to Eq. (1).

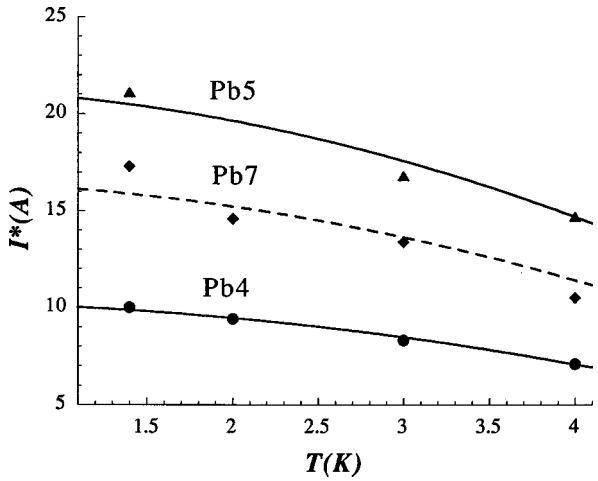

FIG. 5. I^* vs T for Pb samples, fitted to Eq. (7).

The critical field $H_c(T)$ was optically measured as the field at which all the superconducting zones disappear. It is described with enough precision, for the present purposes, by the parabolic law $H_c(T)=H_c(0)[1-(T/T_c)^2]$, with $H_c(0)$ and T_c equal to 800 Oe and 7.19 K for Pb and 30 Oe and 3.77 K for In.

C. Results

1. V-I characteristics and I_c

The V-I characteristics shown in Fig. 3 for sample Pb12 at 4.2 K and different reduced fields $h=H_a/H_c$ are typical of all other samples. The corresponding values of $I_c(h)$ are obtained from these curves from the intersections with the horizontal axis, as indicated in the figure. A common feature observed in all V-I curves, not only in type-I,[19] but also in type-II,[10] samples, is the existence of a point where the extrapolated V-I lines apparently intersect in the third quadrant, as indicated in the figure. Until now we could not decide whether this feature was simply a coincidence favored by measurement uncertainties or if, on the contrary, it was a property related to the geometry of the samples. In Sec. III we will see the theoretical confirmation of the latest option. Let us now see an important implication for $I_c(h)$ arising from this peculiar property.[16]

Let the coordinates of the interception point be $(-I^*, -V^*)$. Then the general equation for the V-I lines is $V+V^*=R(h)[I+I^*]$. From the flux-flow theory we have $R(h)=R_n h$, where R_n is the normal resistance, i.e., for $h=1$. Considering the particular V-I line with $h=1$, evaluated at $V=I=0$, we obtain $V^*=R_n I^*$. Thus setting $V=0$ in the general V-I equation gives

$$I_c(h)=I^*(T)\left(\frac{1}{h}-1\right). \tag{1}$$

Figure 4 shows measured values of I_c vs $1/h$ for some Pb samples with different thicknesses at 4.0 K. All the measured samples follow the law of Eq. (1). From this equation we conclude that the dependence of I_c on the geometry of the sample and temperature is contained in the parameter I^*. Figure 5 shows I^* vs T for three Pb samples, and Fig. 6 presents the dependence of I^* on the thickness of the sample at two temperatures.

In order to see the influence of the shape of the sample's edges on the geometrical barrier, we have one sample (Pb15) with one beveled edge at 30° and another sample (Pb14) with two beveled edges at 30°. Figure 7 shows measured values of I^* vs T for these samples compared with sample Pb16, which has rectangular edges and the same thickness of the others. For sample Pb15 two situations are presented: in Pb15a the direction of I is such that the flux penetrates from the rectangular edge, and in Pb15b I is inverted so that the flux penetrates from the beveled side. First, we observe a reduction in I^* of about 35% from Pb16 to Pb15a. An additional reduction of about 15% occurs in Pb15b. The biggest total reduction, of about 70%, is observed in Pb14, with beveled 30° edges on both sides. These results confirm the existence of a barrier, not only for flux entry, but also for flux exit and the important role played by the shape of the edges, as pointed by Provost *et al.*[13] Another interesting result, related to the influence of the sample's edges, was obtained by measuring the V-I characteristics in the Hg disk for a fixed field. The current was radially flowing between a wire inserted at the center and the return electrode consisting of several wires evenly distributed around the periphery of

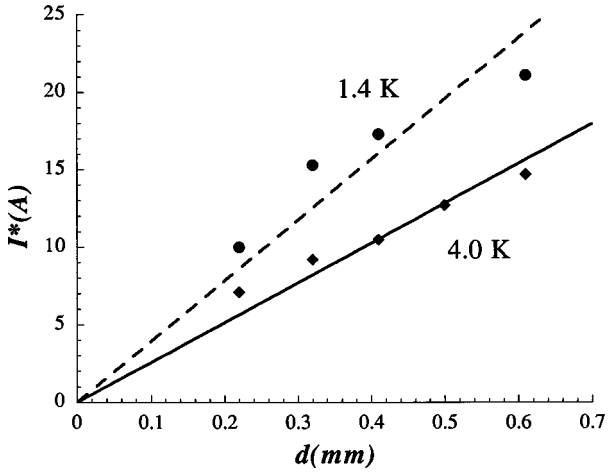

FIG. 6. I^* vs sample thickness d, for Pb samples. Lines are fits to Eq. (7).

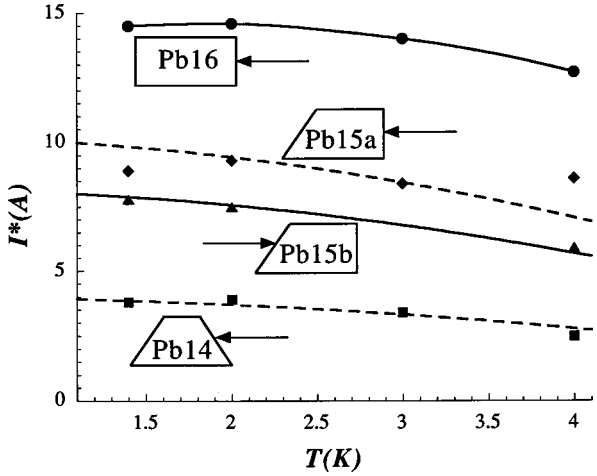

FIG. 7. I^* vs T for Pb samples with different edge shapes. The arrows indicate the direction of flux entry.

the disk. In this configuration, the trapped flux structure turned around the center without having to cross any edge. The result was that all V-I curves for different h passed by the origin, thus giving $I_c(h)\equiv 0$. The potential contacts were located along the same radial line in two different positions.

2. Field for the first flux penetration, H_p

The penetration of the first flux bundles to the center of the strip follows the instant when a reversible curtainlike structure appearing at the edges attains its maximum depth inside the sample. Then, flux bundles start to migrate to the center, escaping from the edge structure.[12] The field at which this happens, H_p, is shown in Fig. 8 for Pb samples at two temperatures. The data are plotted as function of the variable $1/(1+G)$, where the geometrical factor $G=\sqrt{2W/d}$ is the square root of the width to thickness ratio. This result is discussed in Sec. III.

3. Flux-free zones

a. Dependence of the flux-free zone, Δ, on H_a for $I=0$. When $I=0$ the flux distribution inside the strip is symmetric, as in Fig. 2. The field dependence of the width $\Delta(h)$, of the

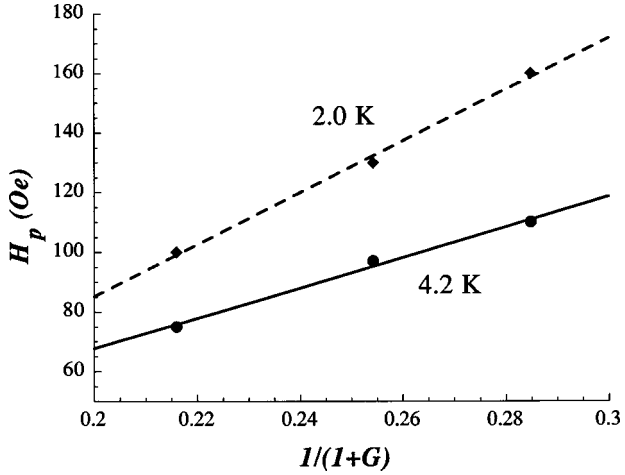

FIG. 8. First-flux penetration field H_p vs the geometry-related variable $1/(1+G)$, where $G=\sqrt{2W/d}$. The lines are fits to Eq. (5).

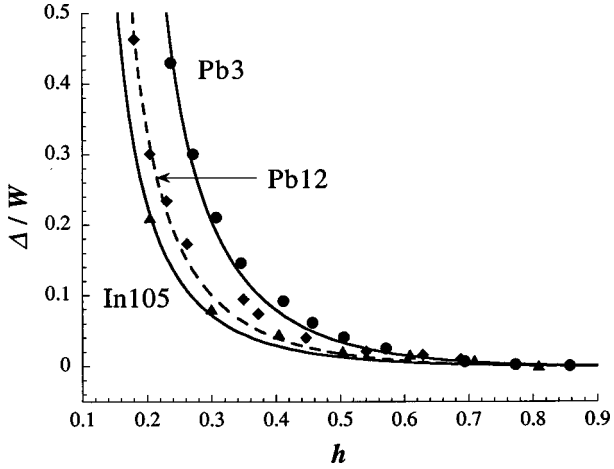

FIG. 9. Width of the symmetric ($I=0$) flux-free zones Δ/W vs h for Pb and In samples. Data for each sample at different temperatures give a single curve.

flux-free zones, normalized by the half width of the strip, W, for two Pb samples and for one In sample is shown in Fig. 9. In this plot the curves measured at different temperatures, for each sample, coalesce into a single one. This is understood from the theoretical discussion in Sec. III, where we see that the temperature dependence of Δ is carried by H_c, already included in h.

b. Dependence of the flux-free zone, Δ, upon I for constant H_a. When H_a is held constant, the flux-free zones change with I in a nonsymmetric way, as illustrated in Fig. 10. For a positively increasing I, the right-hand zone Δ_R rapidly diminishes until it becomes practically zero at $I=I_c$. Simultaneously, Δ_L is only slightly reduced. Figure 11 shows the dependence of Δ_R/W on I at different reduced fields for sample Pb10 at 4.2 K. A similar behavior is observed in all the other samples at different temperatures.

III. THEORY

In this section we summarize some theoretical results from Ref. 15, originally made for type-II superconductors. We have adapted them by simply replacing the first critical field H_{c1} by the critical field H_c of type-I superconductors. This procedure is justified by the similar role these two fields play in the flux penetration process and by the electromag-

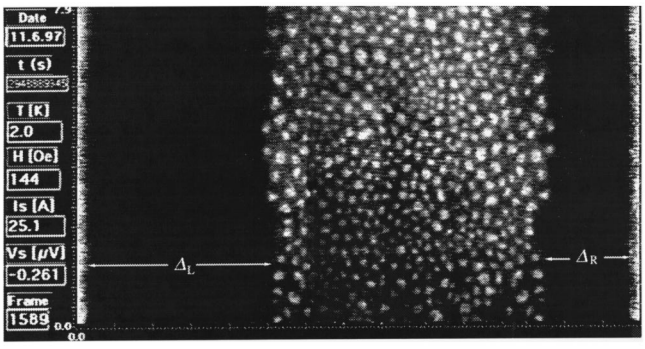

FIG. 10. Magneto-optical image of nonsymmetric flux distribution ($I\neq 0$) for a Pb sample. Δ_R/W decreases with I until it becomes ≈ 0 at $I=I_c$.

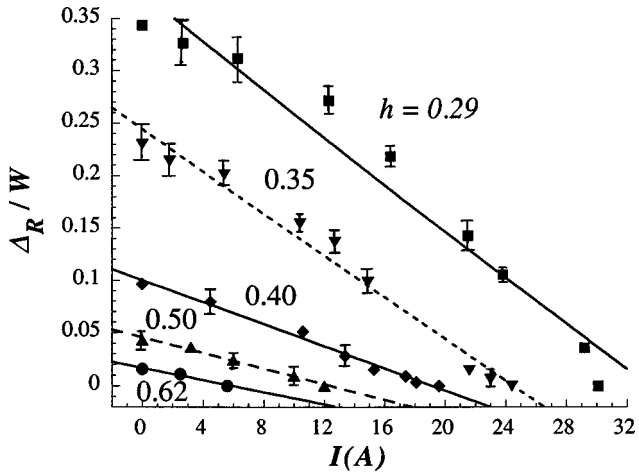

FIG. 11. Width of the nonsymmetric flux-free zone Δ_R/W vs I, for sample Pb10 at 4.2 K, at the indicated reduced fields. Lines are fits to Eq. (3).

netic origin of the studied phenomenon, which makes it depend more on the geometry than on the detailed structure and type of superconductivity. We are aware of certain differences regarding the detailed process of flux penetration and the flux structures in the two cases. Nevertheless, we believe they do not affect the results in the present discussion.

A. Current and flux distributions

Let us consider a type-I superconducting strip of width $2W$ ($-W<x<W$) and thickness d ($-d/2<z<d/2$) with an external field H_a applied along $\hat{z}$ and a transport current I along $\hat{y}$. For $I=0$, at low fields the shielding current extends through the whole sample[9,15] and is gradually confined to the periphery of the strip in a zone that narrows as H_a is increased. The spatially distributed current creates a free-energy gradient, causing a force that pushes the flux lines towards the central axis ($x=0$) of the strip, in opposition to a repulsive force originated on the edge-shape barrier.[9,15] When $H_a \geqslant H_p$ the inwards Lorentz force overcomes the repulsive one, allowing the flux entry. The penetrated flux then occupies the central, current-free zone, whose width gradually increases with H_a, until it fills the whole sample for $H_a \geqslant H_c$. As a result of the absence of volumetric pinning, no current can flow in the central, flux-occupied zone. Conversely, no flux structure can stay on the two lateral zones where the current flows. Figure 2 illustrates the flux distribution in this case.

The general solution for $I \neq 0$ is described by the following current and flux distributions:[15]

$$J_y(x)=\begin{cases} -\dfrac{2xH_a}{|x|d}\sqrt{\dfrac{(x-b_R)(x+b_L)}{W^2-x^2}}, & -W\leqslant x\leqslant -b_L,\quad b_R\leqslant x\leqslant W, \\ 0, & -b_L<x<b_R, \end{cases} \tag{2a}$$

where J_y is the total current density (shielding plus transport contributions) averaged over the thickness of the sample and

$$B_z(x)=\begin{cases} -\dfrac{\mu_0 H_a}{d}\sqrt{\dfrac{(b_R-x)(x+b_L)}{W^2-x^2}}, & -b_L\leqslant x\leqslant b_R, \\ 0, \quad \text{elsewhere inside the sample}, \end{cases} \tag{2b}$$

where B_z is the magnetic induction, and b_R and $-b_L$ are the right and left borders of the flux-occupied zone, so that the widths of the flux-free zones are related by $\Delta_R = W - b_R$ and $\Delta_L = W - b_L$.

B. Critical current and width of flux-free zones

In contrast to the symmetric flux profile, initially existing for $I=0$ (Fig. 2), as I is increased, the flux-occupied region becomes deformed because b_R and $-b_L$ are shifted to the right in different proportions, due to the imbalance of current distributions created by I (Fig. 10). From the condition that the integral of the current density [Eq. (2a)] equal I and the additional requirement that the field at the left edge equal H_c, the following expression is obtained for the width of the flux-free zones:

$$\left.\begin{matrix} \dfrac{\Delta_R}{W} & (-) \\ \dfrac{\Delta_L}{W} & (+) \end{matrix}\right\} = 1 \mp \frac{I}{2\pi W H_a} - \sqrt{\left(1+\frac{I}{2\pi W H_a}\right)^2 - \frac{1}{G^2}(1/h-1)^2}, \tag{3}$$

where the geometric factor $G=\sqrt{2W/d}$. In the case $I=0$, Eq. (3) simplifies to

$$\Delta/W = 1-\sqrt{1-G^{-2}(1/h-1)^2}. \tag{4}$$

The critical current is reached when the following two conditions are fulfilled: $\Delta_R \approx 0$ (flux exit condition) and the field at the left edge $\geqslant H_c$ (flux entry condition). The latter occurs when H_a attains the value

$$H_p = H_c/(G+1). \tag{5}$$

These two conditions lead to the following expression for critical current:

$$I_c(h) = \frac{\pi W H_c}{G^2}\left(\frac{1}{2h}-1\right). \tag{6}$$

IV. DISCUSSION

Comparing the empirical law for I_c vs h of Eq. (1) with the theoretical result of Eq. (6), both look very similar, except for the factor of 2 multiplying h in Eq. (6). The last one incorrectly predicts zero I_c for $H_a = H_c/2$. In this case the theory[15] adapted to type-I superconductors does not work. Nevertheless, this theory explains the physical origin of Eq. (1), confirming this law. Comparing the constant factor in these two equations, we obtain the following expression for I^*:

$$I^*(T) = \left(\frac{\pi d}{2}\right) H_c(T). \tag{7}$$

The data shown in Fig. 5 for I^* vs T differ by a factor of 2–3 from the values calculated using Eq. (7). The increase of the discrepancies with d suggests an incorrect geometric factor. According to Eq. (7), I^* depends linearly on d. However, the data shown in Fig. 6 do not fit the straight lines well, especially at 1.4 K. The slopes of the fitted lines are about 3.5 times the corresponding theoretical values. A better fit to this data is obtained by a power law of d with an exponent of 0.71. The determining role played by the shape of the edges on I^*, demonstrated in Fig. 7 and also explained in Ref. 15, suggests that, in fact, our samples have rectangular edges and not rounded ones as assumed in Ref. 15; this and the fact that in our samples the ratio $d/2W \approx 0.1$ and not really $d/2W \ll 1$ as required by the theory can be important reasons for these disagreements with the theory.

The results plotted in Fig. 8 for H_p confirm the geometric dependence described by Eq. (5), in agreement also with the result in Ref. 13. The slope of these lines is $H_c(T)$ and corresponds correctly to the independently measured value $\approx$530 Oe at 4.2 K. However, the slope of the line at 2.0 K is about 17% smaller than the expected value of $\approx$741 Oe.

The field dependence of Δ/W shown in Fig. 9 is qualitatively well described by Eq. (4). However, calculated values are slightly greater than the experimental data. The solid lines are fits to Eq. (6), where we have replaced G by a fitting parameter whose value is about $1.4G$.

The dependence of Δ_R on I, shown in Fig. 11, corresponds well with the plotted lines at fields $h > 0.5$. At lower fields there is a departure from the lines in the low-current range. We have obtained reasonable numerical agreement between these results and theory (solid lines) by fitting the data to Eq. (3), replacing the geometric factors G and W with two new fit parameters. The final values of the fit parameters were about $1.5G$, consistent with the previous fit, and $2.5W$.

V. SUMMARY

The current and flux distributions in pinning-free strips exposed to a perpendicular magnetic field and a longitudinal transport current present special features related to the geometry of the samples. An energy barrier for flux penetration is originated due to the nonellipsoidal cross section and edge shape of the strips. This so-called geometrical barrier gives rise to a critical current that follows the field dependence of Eq. (1). Its geometric dependence is suggested by Eq. (7), with the minor corrections mentioned in the text. The threshold value of the applied field, at which flux bundles start penetrating to the center of the strip, H_p, is given by Eq. (3), where we observe its geometric dependence.

A visible manifestation of the geometrical barrier is the appearance of two flux-free zones at the edges of the strip. The widths of these zones depend both on the applied field and on the transport current. These dependences are qualitatively well described by Eq. (3). Corrections of the geometric factors, $1.4G$ instead of G and $2.5W$ instead of W, are needed in order to obtain good agreement.

The numerical discrepancies found between experiment and theory are attributed to incorrect geometric factors. This is probably due to the different edge shape, rectangular in our samples, in contrast to the rounded ones assumed in the theory. Furthermore, the required condition $d/2W \ll 1$ of the theory might not be sufficiently satisfied in our samples, where this ratio is about 0.1.

In conclusion, the theory of Ref. 15 describes qualitatively well the observed manifestations of the geometrical barrier, enhancing the present understanding of this phenomenon. However, we point out the need for a revision of this theory concerning the geometric factors and the particularities of type-I superconductors.

ACKNOWLEDGMENTS

We want to thank Dr. I. L. Landau for helpful discussions and advice during the realization of the experiments and this report. We thank Professor R. Huguenin and Professor R. Rosenbaum for helpful comments, and Dr. M. Lampert for correcting the English of the final manuscript. We thank especially Professor J. R. Clem for kindly sending us his manuscript[15] before publication. This work was partially financed by the Swiss National Science Foundation.

*Present address: School of Physics and Astronomy, Tel Aviv University, 69978 Tel Aviv, Israel.

†Present address: Department of Electrical Engineering, Swiss Federal Institute of Technology, CH-1015 Lausanne, Switzerland.

‡Present address: Institut Suisse de Meteorologie, CH-1530 Payerne, Switzerland.

[1] E. H. Brandt and M. Indenbom, Phys. Rev. B **48**, 12 893 (1993).

[2] L. Burlachkov, Phys. Rev. B **47**, 8056 (1993).

[3] V. Kogan, Phys. Rev. B **49**, 15 874 (1994).

[4] Y. Mawatari and K. Yamafuji, Physica C **288**, 336 (1994).

[5] N. Chikumoto, M. Konczykowski, N. Motohira, and A. Malozemmoff, Phys. Rev. Lett. **69**, 1260 (1992).

[6] V. Kopilov, A. Koshelev, I. Schegolev, and T. Togonizde, Physica C **170**, 291 (1990).

[7] L. Dorosinskii, V. Nikitenko, and A. Polyanskii, Phys. Rev. B **50**, 501 (1994).

[8] M. McElfresh, Y. Yeshurun, A. Malozemoff, and F. Holtzberg, Physica A **168**, 308 (1990).

[9] E. Zeldov, A. Larkin, V. Geshkenbein, M. Konczykowski, D. Mayer, B. Khaykovich, and V. Vinokur, Phys. Rev. Lett. **73**, 1428 (1994).

[10] R. Huebener and R. Kampwirth, J. Low Temp. Phys. **2**, 113 (1979).

[11] A. Larkin and Y. Ovchinnikov, Sov. Phys. JETP **34**, 651 (1972).

[12] A. Fortini and E. Paumier, Phys. Rev. B **14**, 55 (1976).
[13] J. Provost, E. Paumier, and A. Fortini, J. Phys. F **4**, 439 (1974); A. Fortini, A. Haire, and E. Paumier, Phys. Rev. B **21**, 5065 (1980).
[14] E. Zeldov, J. R. Clem, M. McElfresh, and M. Darwin, Phys. Rev. B **49**, 9802 (1994).
[15] M. Benkraouda and J. R. Clem, Phys. Rev. B **53**, 5716 (1996); **58**, 15 103 (1998).
[16] B. Dutoit, Ph.D. thesis, IPE Lausanne University, Lausanne, Switzerland, 1995.
[17] B. Dutoit and L. Rinderer, Jpn. J. Appl. Phys., Suppl. **26**, 26-3 (1987).
[18] H. Kirchner, Phys. Lett. **30A**, 437 (1969).
[19] B. Dutoit and L. Rinderer, Helv. Phys. Acta **62**, 886 (1989).